NASA TECHNICAL NOTE

NASA TN D-3279

NASA TN D-3279
c. 1
LOAN COPY: R
AFWL (W
KIRTLAND AF
0079791
TECH LIBRARY KAFB, NM

A PHOTOVOLTAIC SOLAR SENSOR FOR USE IN SPACECRAFT ORIENTATION CONTROL SYSTEMS

by Anthony Fontana

Langley Research Center

Langley Station, Hampton, Va.

NATIONAL AERONAUTICS AND SPACE ADMINISTRATION • WASHINGTON, D. C. • FEBRUARY 1966

TECH LIBRARY KAFB, NM
0079791

NASA TN D-3279

A PHOTOVOLTAIC SOLAR SENSOR FOR USE IN SPACECRAFT ORIENTATION CONTROL SYSTEMS

By Anthony Fontana

Langley Research Center
Langley Station, Hampton, Va.

NATIONAL AERONAUTICS AND SPACE ADMINISTRATION

For sale by the Clearinghouse for Federal Scientific and Technical Information
Springfield, Virginia 22151 – Price $2.00

A PHOTOVOLTAIC SOLAR SENSOR FOR USE IN SPACECRAFT ORIENTATION CONTROL SYSTEMS*

By Anthony Fontana
Langley Research Center

SUMMARY

A simple photovoltaic solar sensor has been designed, constructed, extensively ground tested in simulated space environments, and space tested during a suborbital flight. The sensor has the capability of solar capture from any initial orientation within its spherical field of view and the capability of accurate pointing toward the solar target without the introduction of error by earth-reflected solar radiation. The sensor has a repeatability of ±2.4 seconds of arc at a pointing error of 1 minute of arc. The sensitivity and linear range of the sensor are adjustable. State-of-the-art protection from space radiation degradation is provided. The sensor is conservatively estimated to have an earth-orbit lifetime of 10 years with no more than 10-percent degradation.

INTRODUCTION

A solar sensor can be defined as a device having an electrical output which provides sufficient information to allow the determination of both the magnitude and direction of the instantaneous angular pointing error of the null axis of the sensor relative to the solar vector. That is, a solar sensor is a device which, when used as an input to an attitude control system, provides for the orientation of a specified axis of a spacecraft toward the center of the solar disk.

In the future, as has been in the past, the degree of success attained in various space missions will depend on the reliability and performance of the simple photovoltaic solar sensor. The photovoltaic solar sensor is inherently reliable and has sufficient accuracy for use in space missions which require solar orientation for the purpose of converting the radiant energy of the sun to electrical power, solar orientation for the purpose of solar observation and study, solar sensing for the purpose of obtaining an interplanetary navigational reference, and solar orientation for temperature balance. Among the major projects which require the use of solar sensors for either solar observation or navigational references are Orbiting Solar Observatory, Orbiting

*The information presented herein was prepared for submission as a thesis in partial fulfillment of the requirements for the degree of Master of Electrical Engineering, University of Virginia, Charlottesville, Virginia, October 1965.

Geophysical Observatory, Ranger, Mariner, Surveyor, and Lunar Orbiter. These projects have a combined total of over 50 earth-orbit, lunar-orbit, lunar-probe, and planetary-probe missions scheduled between 1965 and the mid 1970's.

In view of the apparent continuing need for the photovoltaic solar sensor, it is appropriate that a general purpose photovoltaic solar sensor has been designed and constructed. The purpose of this paper is to describe this general purpose solar sensor, which has simple but unique design, construction, and operation, enabling it to satisfy the requirements of present space missions with respect to simple solar sensors.

A photovoltaic solar sensor, which was similar to the general purpose sensor described herein, was space flight tested as part of NASA's Spacecraft Orientation Control Systems (SOCS) Project in September 1963. The sensor survived the rugged launch environment and functioned properly during the 7-minute ballistic test period. A complete description of the Project SOCS spacecraft and a detailed analysis of the flight test results are presented in reference 1.

SYMBOLS

Measurements in this report are given in the SI system with the exception of nautical miles. To convert nautical miles to kilometers, the value of the U.S. Customary Unit was multiplied by 1.85.

g	force of the earth's gravitational field per unit mass
I_{sc}	instantaneous short circuit current of a silicon solar cell
$I_{sc,o}$	initial short circuit current of a silicon solar cell
N/P	negative semiconductor on positive semiconductor
P/N	positive semiconductor on negative semiconductor
s	shielding, grams per square centimeter
α	half-angle field of view of the fine sensor, degrees
θ	the angular pointing error caused by earth-reflected solar radiation, degrees
θ_{max}	the maximum angular pointing error caused by earth-reflected solar radiation at a specific altitude, degrees
Φ	electron flux, electrons per square centimeter per day
Ψ	angle formed by the earth-sun line of centers and the line from the center of the earth to the sensor, degrees

DESCRIPTION

A drawing of a test model solar sensor is shown in figure 1. It is actually a dual sensor composed of coarse sensing elements, used during target capture maneuvers from large initial error angles, and fine sensing elements,

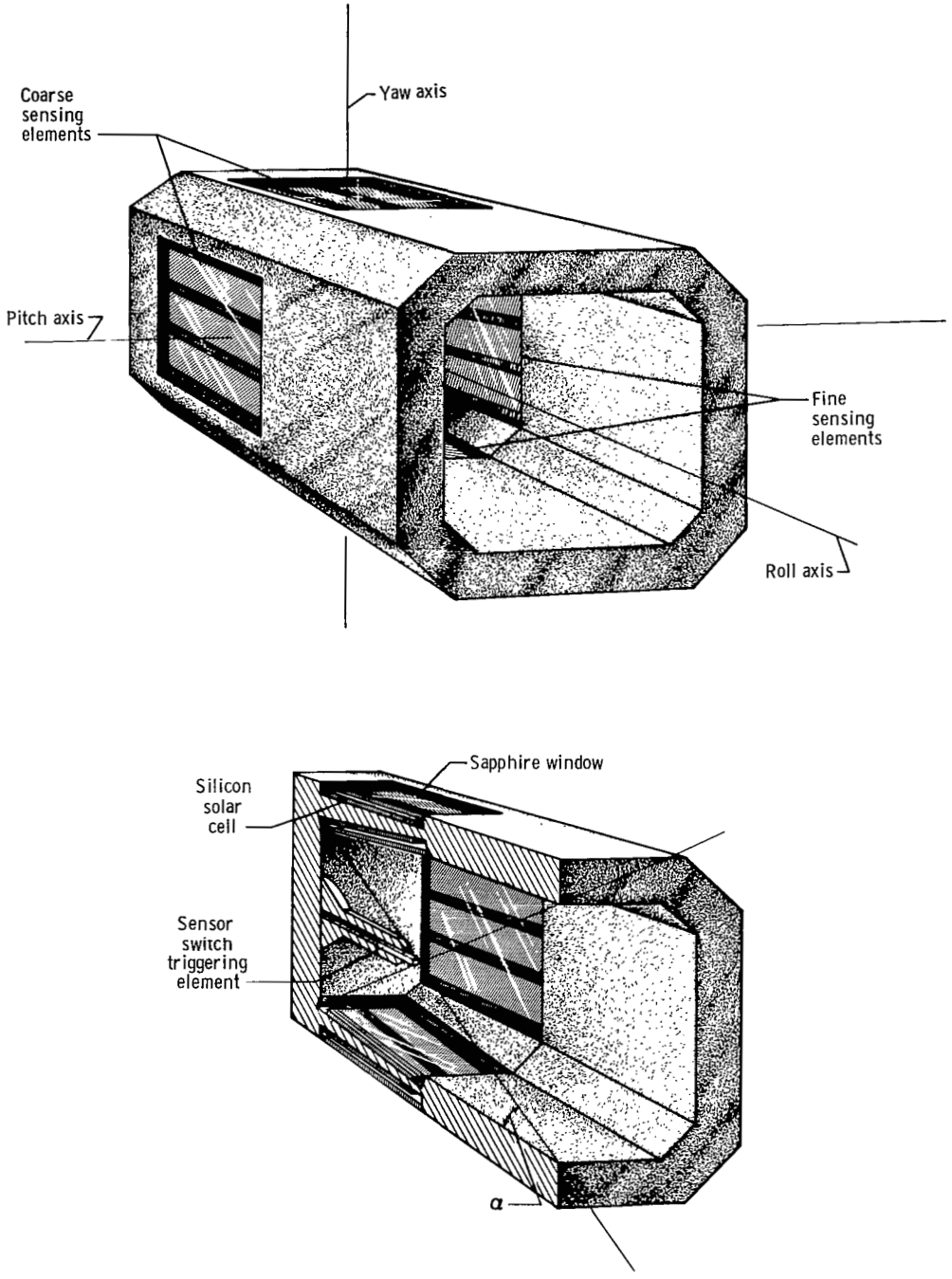

Figure 1.- Drawing of a solar sensor.

used during accurate pointing. The sensing elements are composed of silicon solar cells connected in series. Geometrically opposing coarse sensing elements and geometrically opposing fine sensing elements are electrically connected in a battery bridge circuit, as shown in figure 2, for the purpose of obtaining a sensor output with an electrical polarity which indicates the direction of the pointing error. The coarse sensing elements located in both the pitch and yaw axis provide the sensor with a full spherical field of view and thus the capability of capturing the solar target from an initial error angle of 180°. It should be noted at this point that, whereas the sensor shown in figure 1 is adequate for test purposes, in an actual space mission the four coarse sensing elements must be located at 90° intervals on the outer extremes of the payload so that the field of view of the coarse sensor is not obstructed by any part of the payload.

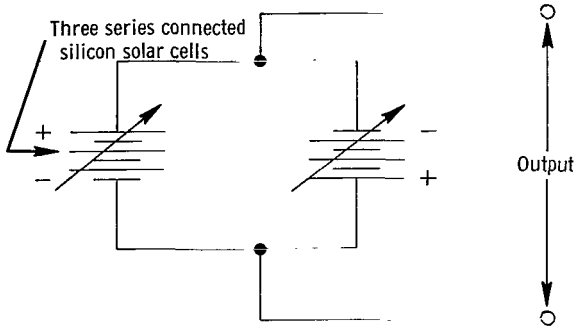

Figure 2.- Schematic diagram of a single sensing element.

To examine the need for a dual solar sensor, a spacecraft equipped with an attitude control system and a coarse sensor is assumed to be in orbit about the earth and to be oriented with respect to the earth and sun as shown in figure 3. The sensor, having a spherical field of view, will be able to observe both the earth and sun simultaneously. Since the earth reflects a great deal of solar radiation, the sensor actually sees two sources of radiation and will require

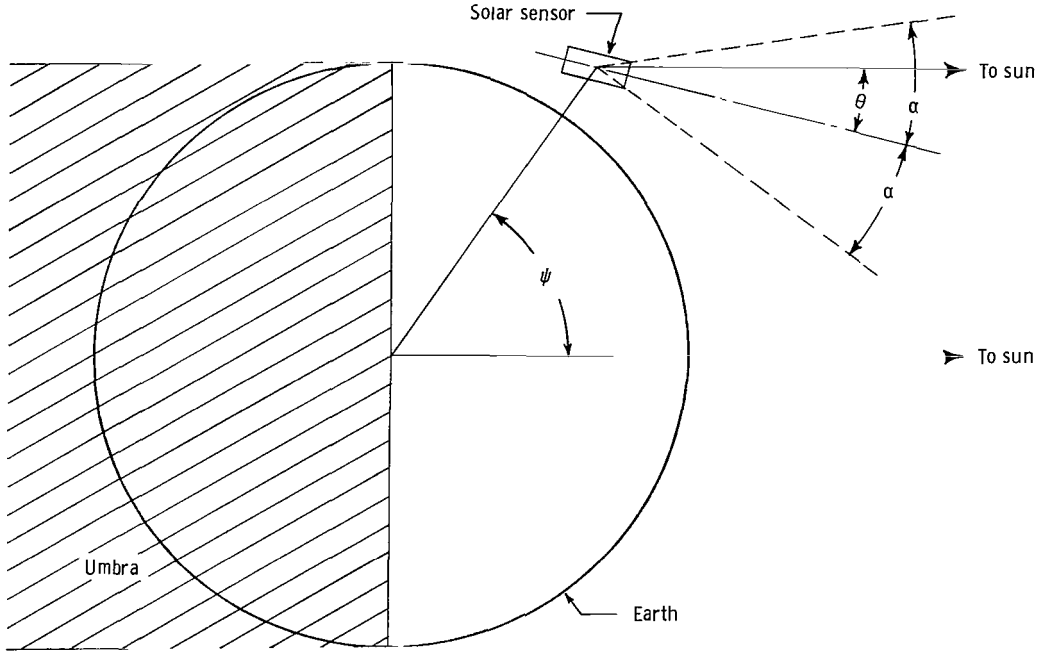

Figure 3.- Effect of earth-reflected solar radiation on solar sensing.

that the spacecraft orient itself toward some point between the two sources; this orientation is dependent upon the angular separation and relative intensities of the radiation sources. Therefore, an angular pointing error θ (see fig. 3) will exist with respect to the solar vector because of earth-reflected solar radiation. If the field of view of the assumed sensor is limited to the conical angle α (see fig. 3), the sensor can no longer observe both the earth and the sun simultaneously. Thus, when oriented toward the sun, the sensor is unable to see the earth, and its pointing accuracy is unaffected by earth-reflected solar radiation.

The preceding discussion establishes the need for a dual sensor composed of coarse sensing elements, which have the full spherical field of view necessary to provide capture capability from large error angles, and fine sensing elements, which have a field of view limited to the extent that the pointing accuracy is unaffected by earth-reflected solar radiation. Reference 2 sets forth the basic concepts of a dual sensor and presents a mathematical description of the pointing error caused by earth-reflected solar radiation as a function of the geocentric angle ψ and the altitude of the sensor. The formula derived in reference 2 was used to calculate the relation between the pointing error caused by earth-reflected solar radiation θ and the geocentric angle ψ

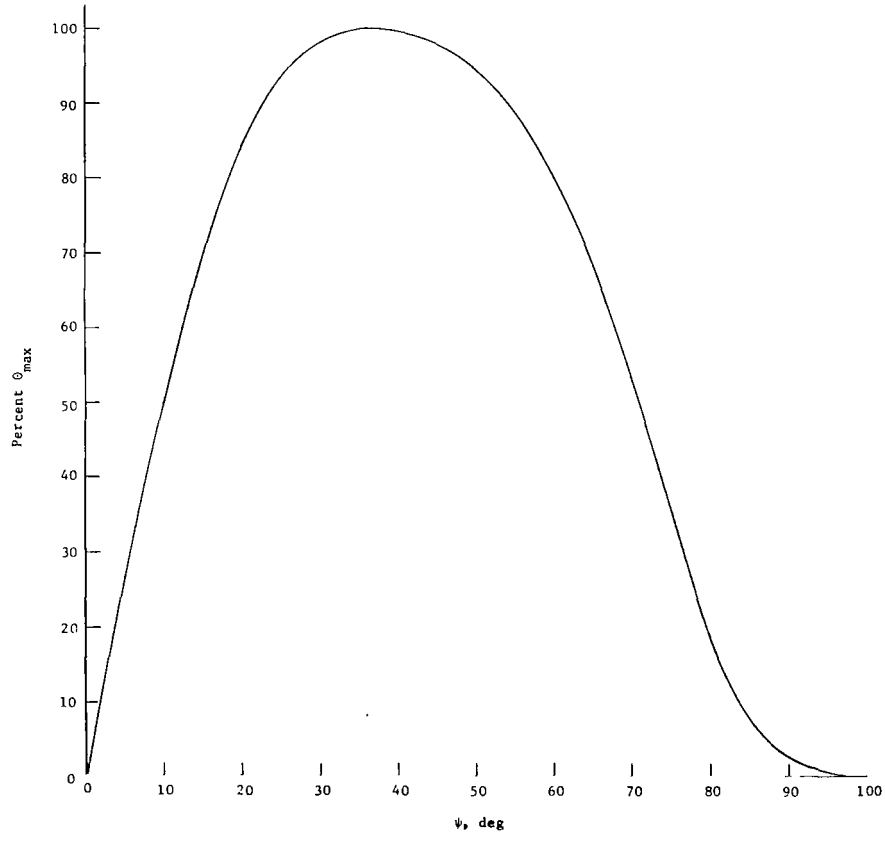

Figure 4.- Angular pointing error introduced by earth-reflected solar radiation.

shown in figure 4. Although the relation presented in figure 4 is for a specific altitude of 300 nautical miles (555 kilometers), the shape of the curve is typical.

It should be noted that regardless of the limitation of the angular field of view of the fine sensor, pointing errors due to earth-reflected solar radiation will always occur when the sun appears to be near the earth horizon, that is, when the geocentric angle is near 90°. However, as shown in figure 4, the pointing error due to earth-reflected solar radiation decreases rapidly as the geocentric angle approaches 90°. While the sun is within α degrees of the earth horizon, the extent to which the fine sensor output is usable will depend upon the mission parameters (such as orbit inclination and altitude in the case of earth orbits) and the absolute solar pointing accuracies required.

The preceding discussion has been concerned with the earth as a source of reflected solar radiation, but the concepts involved apply to the albedo of any planetary body or natural satellite that becomes significant during interplanetary or lunar missions.

The boundary of the conical angle α (see fig. 1) serves as the triggering point for an electronic circuit which switches from the coarse sensing elements to the fine sensing elements. In order to insure capture of the solar disk, the switching angle (equal to α) must be greater than the maximum pointing error angle θ_{max}, where θ_{max} is established by the mission parameters. At the instant the pointing error becomes equal to the switching angle, the sensor-switch triggering element, which is a photoconductive diode, is illuminated by solar radiation and its internal resistance is changed from a nominal value of 1000 megohms to a nominal value of 1000 ohms. This change in internal resistance of the photoconductive diode can be used to trigger the electronic switching circuit.

The composite output characteristic of the single-axis solar sensor is shown in figure 5. The sensor output is derived from the fine sensing elements for pointing errors from zero to $\pm\alpha^{\circ}$ and from the coarse sensing elements for pointing errors from $\pm\alpha^{\circ}$ to $\pm 180^{\circ}$. The slope of the output obtained from the fine and coarse sensing elements is controlled by the load and by optical coatings that are deposited on the inside of the sapphire windows. A detailed description of these optical coatings and the construction of sensing elements is given in a later section of this paper.

The continuous slope of the sensor characteristic makes it convenient to add a damping signal to the sensor output through the use of simple resistance-capacitance lead networks. Damping, and thus stable control, can be provided from zero to $\pm 90^{\circ}$ of pointing error by two lead networks, one connected to each axis of the sensor. Separate lead networks are recommended for use in conjunction with the fine and coarse sensing elements to compensate for the possible difference in the slopes of their outputs. The resistance and capacitance values of the lead networks depend upon the magnitude of the controlling torque and input impedance of the control system with which the sensor is being used and upon the total inertia of the vehicle being oriented.

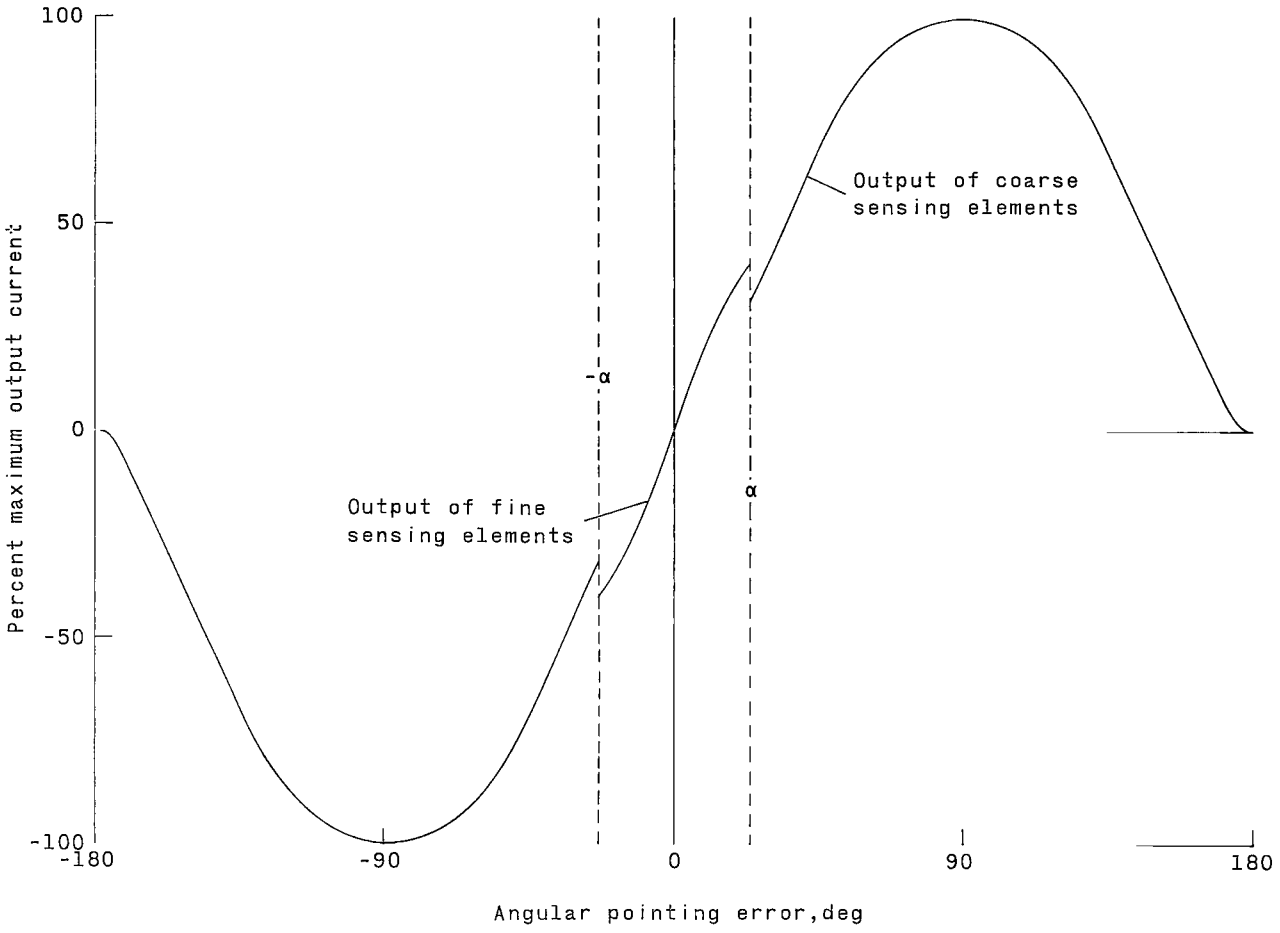

Figure 5.- Single-axis solar sensor output characteristic.

The wide angular range through which a damping signal is available at the sensor output terminals allows the properly adjusted attitude control system to damp out initial angular rates which might be introduced by the launch vehicle. Also the angular momentum built up by the control system itself while capturing from a large error angle can be damped out.

ENVIRONMENT

The solar sensor must be capable of surviving both the space environment and the environment created by the launch vehicle.

Space Environment

Since the ionizing radiation of the near earth space environment is generally more dense than that of interplanetary space, the space environment

usually encountered by earth orbiting spacecrafts will be the environment considered in this paper. The greatest hazard of the earth orbit environment to semiconductors is the electron and proton belts which are geomagnetically maintained in the earth's magnetosphere. Semiconductor damage, which is caused by solar flare proton storms, galactic cosmic rays, solar X-rays, gamma rays, and micrometeoroids, is of secondary importance but will be indirectly considered in the discussion which follows.

Effects of degradation.- Degradation of the silicon solar cells, which form the solar sensing elements of the sensor, by ionizing radiation will be evidenced by a reduced sensitivity only or by a combination of reduced sensitivity and null shift of the sensor output. Reduction of the sensitivity only indicates equal degradation of the two opposing sensing elements but does not alter the ability of the sensor to indicate zero pointing error or to provide an output which can be accurately used by the orientation control system of a spacecraft. A reduced sensitivity does, however, reduce the accuracy with which angular measurements can be made by the sensor. The occurrence of a null shift along with reduced sensitivity indicates unequal degradation of the opposing sensing elements and reduces the accuracy of both the indication of zero pointing error and the angular measurements. Both the reduction of the sensitivity and the null shift of the output are highly undesirable and must either be eliminated or be confined to a tolerable limit.

Angular measurements can not be accurately made by the coarse sensor since its output is contaminated by earth-reflected solar radiation; therefore, degradation of the coarse sensor is relatively unimportant and the following discussion of radiation protection will be confined primarily to the fine sensor. Also, the following discussion is based on a fine sensor field of view of 25° ($\alpha = 25^{\circ}$).

Radiation protection.- Radiation protection for the solar sensor is obtained through proper geometric design, the use of sapphire cover windows for the sensing elements, the selection of the proper type of cell, the selection of an appropriate cell base material resistivity, the use of optical coatings on the cover windows, and preirradiation of the solar cells.

Geometric design: The geometric design of the fine sensor provides the majority of the radiation protection for the fine sensing elements by limiting the field of view to only 6 percent of 4π steradians, or in other words, by limiting the radiation dosage rate to 6 percent of the omnidirectional space radiation dosage rate. The preceding assumes that the fine sensor block provides perfect protection throughout the remaining 94 percent of 4π steradians, which in turn implies an infinitely thick shield. The fine sensors have thus far been constructed of aluminum which has a density of approximately 2.7 g/cm^3 and which at an average thickness of 0.625 cm offers a shielding of 1.7 g/cm^2. A shielding of 1.7 g/cm^2 is effectively infinite for short-duration space missions, but for extended-duration space missions, steel at a density of approximately 8.0 g/cm^3 and an average thickness of 0.625 cm offers the more adequate shielding of 5 g/cm^2.

Cover windows: The second deterrent to radiation damage of the sensing elements is the cover windows which are mounted directly over the silicon solar

cells. (See fig. 1.) The cover window material is artificial sapphire and was chosen because of its resistance to degradation in a radiation environment (ref. 3) and because of its relatively high density as compared to the glasses. The actual thickness of the sapphire windows is 0.15 cm, but, because of the 10° mounting angle of the fine sensing elements and the limited field of view, the solar radiation has an average angle of incidence with the sapphire windows of 67.5° which gives an average effective window thickness of 0.392 cm. Artificial sapphire has a density of 4.0 g/cm^3 and at a thickness of 0.392 cm provides a shielding of 1.57 g/cm^2.

In order to evaluate the effectiveness of the sapphire windows in reducing the radiation damage of the sensing elements, it is necessary to draw from the data generated by recent space and ground research relative to the radiation damage in semiconductor materials. The Telstar I experiment is one of the most thorough combinations of both space and ground studies of semiconductor radiation damage available (ref. 4) and in the interest of simplicity and expediency this Telstar data will be used in the following evaluation of the cover windows.

Telstar had on board several radiation damage experiments, which consisted of N/P silicon solar cells protected by sapphire windows of various thicknesses, in addition to the main power supply, which was made up of N/P silicon solar cells of the same production lot and which was protected by 0.075-cm thick sapphire covers. It is realized that the damage rate data obtained from these Telstar experiments applies only to the Telstar orbit; but, since this orbit had an apogee of 3043 nautical miles (5630 kilometers), a perigee of 512 nautical miles (947 kilometers), and an inclination of 44.8°, the satellite traversed the heart of the inner Van Allen Belt and thus the radiation dosage rate encountered represents a conservative average. By comparing the space experiment data with that data obtained from the ground irradiation of N/P silicon solar cells of the same production lot with 1 MeV electrons, it is possible to determine the 1 MeV electron flux that will produce an equivalent damage rate in N/P solar cells protected by a given shielding. The solid curve of figure 6 is the actual Telstar I data and the dashed extension is extrapolated data (ref. 5). The other curve is plotted from the equation

$$\text{Equivalent 1 MeV electron flux} = 1.04 \times 10^{12}\left(s^{-1.5}\right) \text{ electrons}/\text{cm}^2/\text{day}$$

where s is the shielding in grams per square centimeter. Because of its close correlation with the Telstar I data, this equation is used to extend the Telstar data into the range of shield thicknesses which are of interest relative to the solar sensor. Figure 6 establishes the fact that, at a shielding of 1.57 g/cm^2, 5.3×10^{11} 1 MeV electrons/cm^2/day will produce a damage rate which is equivalent to the damage rate produced by the ionizing radiation of the space environment. The importance of the preceding will be illustrated later in this paper.

Cell type: In striving to achieve the ultimate in resistance to radiation damage, the selection of the type of silicon solar cell becomes important. Silicon solar cells of the N/P type have been conclusively proven to be more resistant to radiation damage than P/N silicon solar cells (ref. 3).

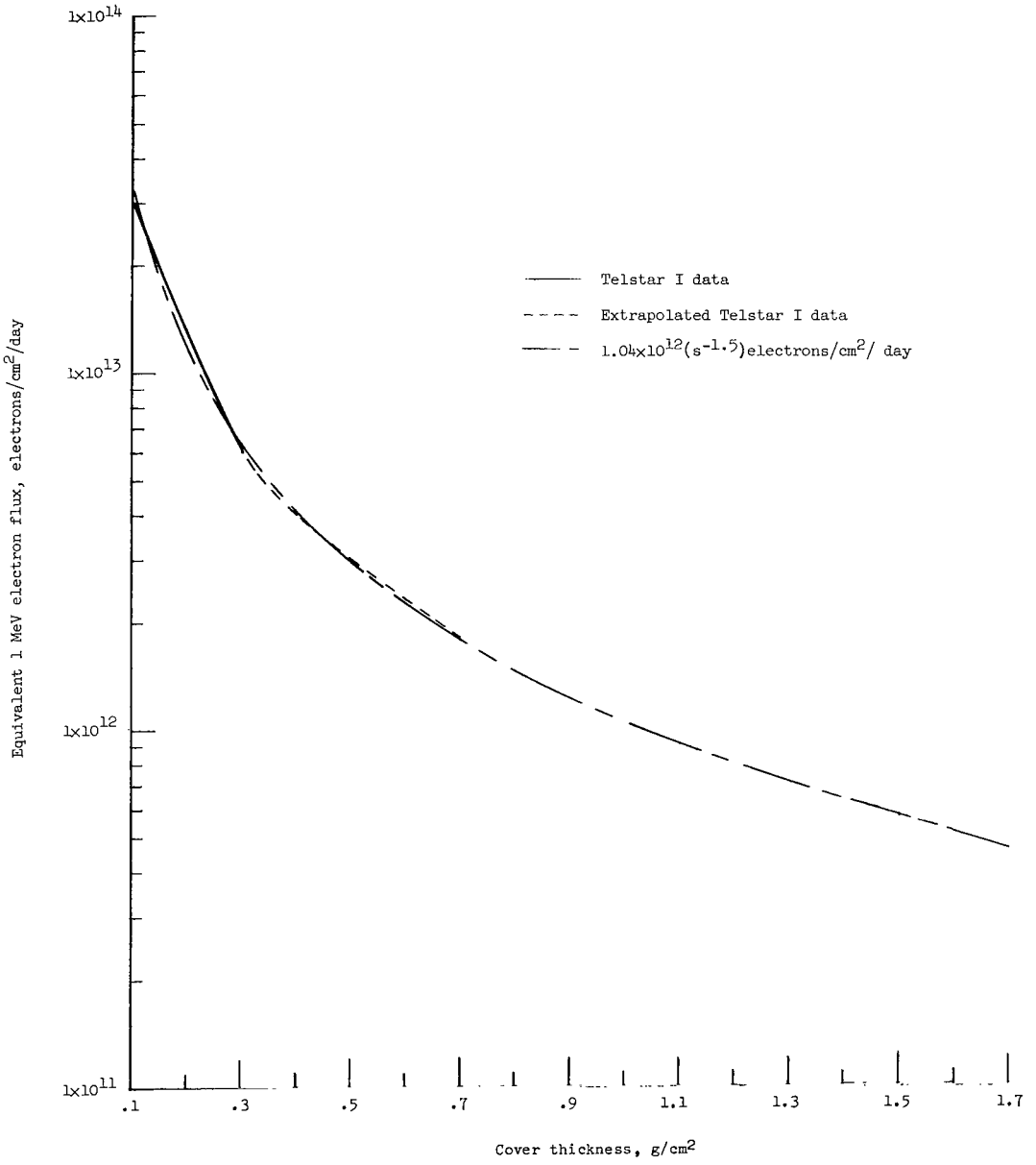

Figure 6.- The 1 MeV electron flux space damage rate equivalent in N/P solar cells.

Base material resistivity: The resistivity of the base material must also be considered when selecting the solar cell most resistant to radiation damage. Figure 7 was taken from reference 6 and shows that silicon solar cells with higher base-material resistivity are more resistant to radiation damage than those cells with lower base-material resistivities. The drift field base material and those base materials with a resistivity greater than 10 ohm-cm are currently experimental. Although it is possible to obtain cells with these experimental base materials in the limited numbers required for the construction of solar sensors and although the use of these cells is recommended, production cells with a base material resistivity of 10 ohm-cm have been used in the sensor described herein.

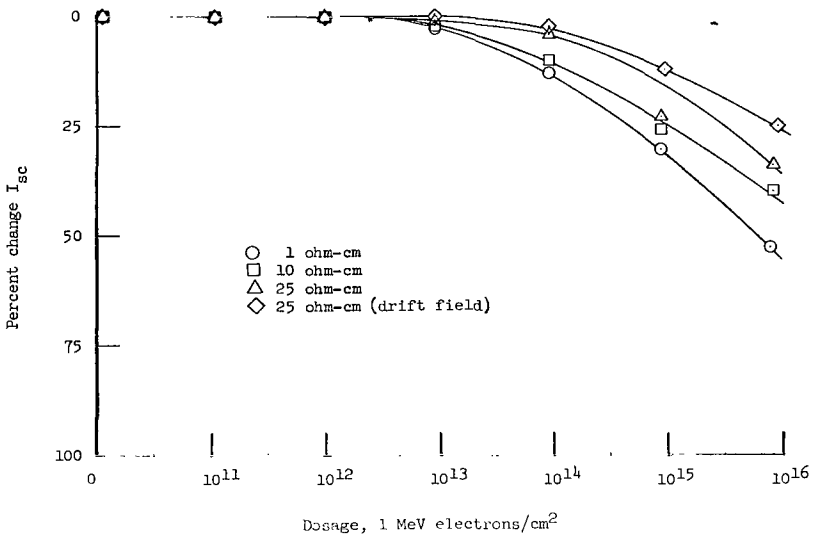

Figure 7.- Comparison of base resistivity with percent change in short circuit current caused by 1 MeV electrons.

Optical coatings: The spectral response of a silicon solar cell degrades much more with irradiation at the longer wavelengths than at the shorter wavelengths. Therefore, through the use of a commercially available optical coating (which can be vacuum-deposited in multilayers on the inside of the sapphire cover windows) the longer wavelengths of solar radiation to which the cells respond can be reflected, thus the effective amount of degradation can be reduced. The degradation of the spectral response of an N/P silicon solar cell with 1 MeV electron irradiation is shown in figure 8 (ref. 3). Superimposed upon the spectral response curves is the transmission curve of the optically coated cover window. By using the curves presented in figure 8, it can be calculated that without the optical coating the silicon solar cells will have degraded approximately 50 percent after a dosage of 1×10^{16} electrons/cm^2, whereas, with the optical coating the cells will have in effect degraded only approximately 25 percent after a dosage of 1×10^{16} electrons/cm^2. Thus, when subjected to equivalent amounts of radiation, the solar sensor equipped with these optical coatings can be expected to degrade only 50 percent of the amount a sensor not so equipped would degrade.

The general purpose solar sensor will operate at angles of incidence between 55° and 80°. The transmission curve of the cover window and optical coating combination of figure 8 was measured at a normal angle of incidence. As the angle of incidence increases, the transmission will decrease and the transmission curve will shift toward the ultraviolet end of the spectrum. At

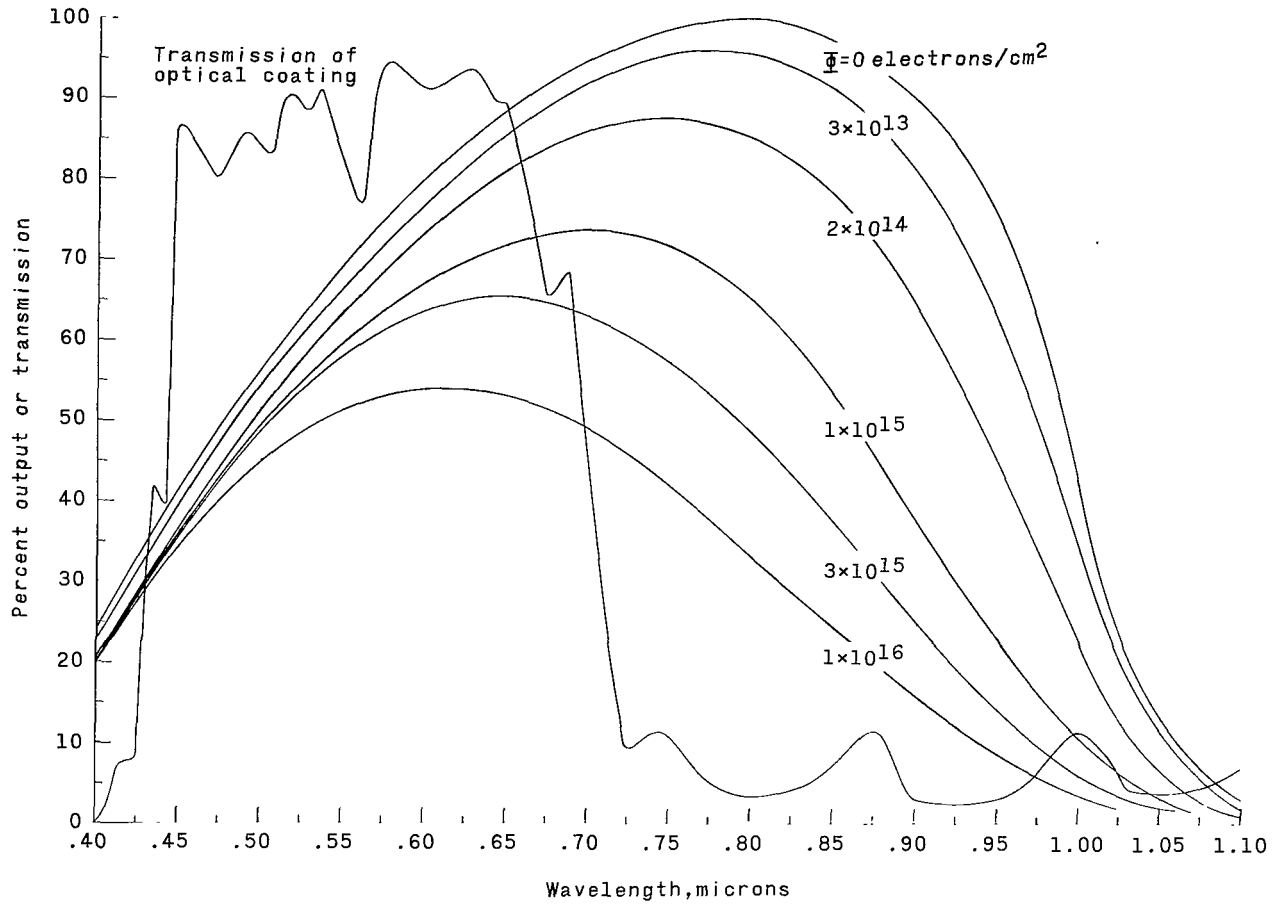

Figure 8.- Reduction of effective degradation of silicon solar cells through the use of optical coatings.

an angle of incidence of 60°, the transmission will have decreased approximately 10 percent and the curve will have shifted approximately 20 millimicrons toward the ultraviolet. As the angle of incidence approaches 80°, the transmission will continue to decrease but the spectral shift will remain near 20 millimicrons. The variation of the transmission with angle of incidence does not significantly alter the factor by which the degradation of the solar sensor is reduced by the use of the optical coating since the shape of the transmission curve does not change appreciably. The shift of the transmission curve toward the ultraviolet end of the spectrum is negligible with respect to the calculation of the factor by which the degradation of the sensor is reduced by the use of the optical coating.

Preirradiation: Probably the most effective and powerful technique for increasing the resistance of a silicon solar cell to radiation damage is that of preirradiation. The silicon solar cell degrades exponentially at higher dosages as shown in figure 9 (ref. 6). Figure 9 is a typical degradation curve for an N/P silicon solar cell that has a base material resistivity of 10 ohm-cm when irradiated by 1 MeV electrons. The data presented in table I

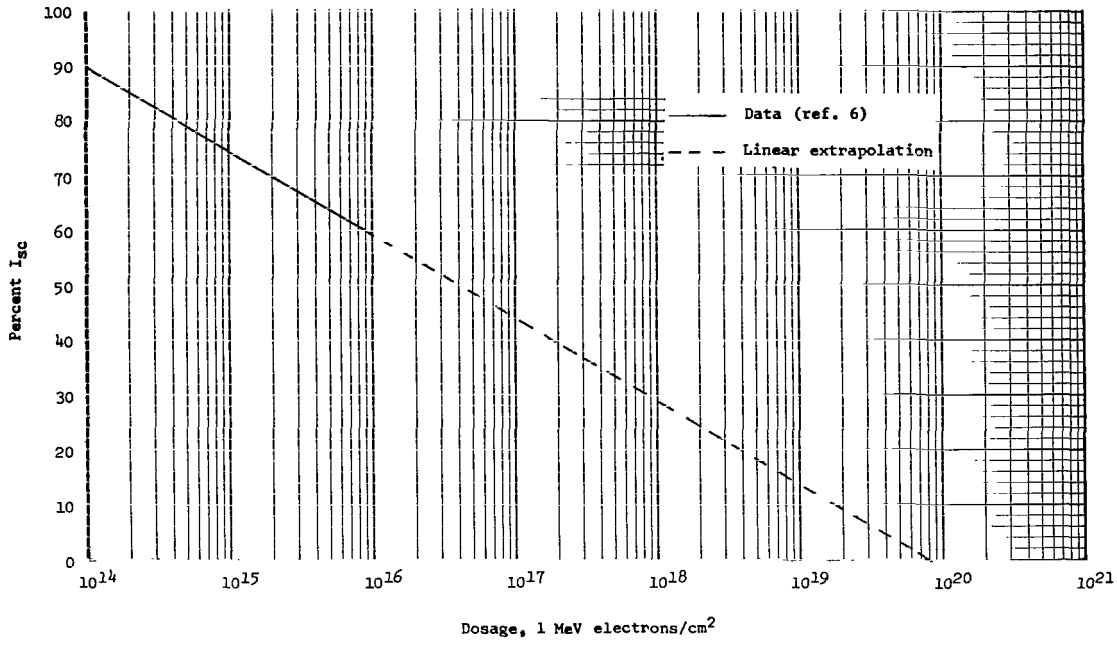

Figure 9.- Typical degradation of a 10 ohm-cm N/P silicon solar cell by 1 MeV electrons.

were taken from figure 9 and illustrate the advantage to be gained with the preirradiation technique. These data show that the 1 MeV electron radiation required to degrade the solar sensor from 20 percent to 10 percent of its original output is five orders of magnitude greater than that required to degrade the sensor from 100 percent to 90 percent of its original output.

A secondary, but important, advantage of the preirradiation technique is the opportunity of matching the degradation rates of the silicon solar cells. It has been established that solar cells which initially degrade equal amounts for a given radiation dosage tend to continue to degrade equally at higher radiation dosages. Therefore, during the process of preirradiating solar cells, it is convenient to set aside pairs of cells which have shown equal degradation rates. By placing one member of a matched pair in one sensing element and the other member in the opposing sensing element, it is possible to insure that the opposing sensing elements will degrade approximately equally in the space environment; thus, the possibility of null shift in the output of the solar sensor can be significantly decreased. The extent to which the null shift of the sensor is lessened by degradation rate matching of the solar cells depends on the accuracy of the matching process. Presently, the available solar cell degradation information is based on data points too widely spaced to permit a detailed analysis of the slope variations of the degradation curves. However, the available degradation information, having data points spaced at dosages differing by one order of magnitude (ref. 6), is sufficient to state that solar cells can be matched during preirradiation to the extent that the divergence from their original slope will not be greater than 2 percent during future exposure to damaging radiation which produces an additional 10-percent drop in

the short circuit current of the cell. The latter statement has not been verified beyond a total degradation of 40 percent of the initial short circuit current.

Electrical load: The electrical load placed on the solar sensor has a significant effect upon the radiation damage rate of the sensor. Figure 10 was taken from reference 7 and shows that the open-circuit voltage of a silicon solar cell degrades only approximately 12 percent, whereas the short-circuit current degrades approximately 45 percent. Thus, the solar sensor which is operated near open circuit will degrade only 27 percent of the amount that a sensor which is operated near short circuit will degrade for an equivalent radiation dose.

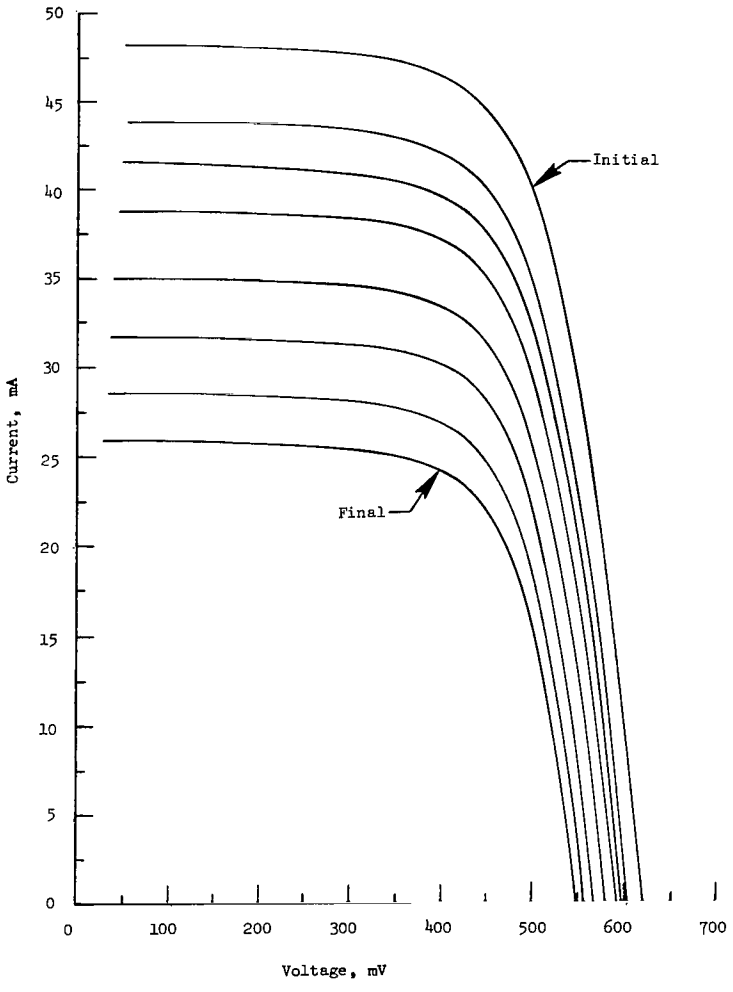

Figure 10.- Typical current-voltage characteristics of a silicon solar cell at various stages of irradiation.

The significance of these seven techniques for the reduction of the radiation damage to the fine solar sensor (i.e., geometric design, sapphire cover windows, type of cell, cell resistivity, optical coatings, preirradiation, and loading) is illustrated in the appendix where the contribution of each technique is calculated.

Operating temperature.- In general, the output of solar cells decreases with increasing cell temperature. Because of this relationship between output and temperature, the sensitivity of the solar sensor can be increased by operating the sensing elements at a low temperature. Thermal protection for the sensing elements can be obtained through the use of optical coatings which are deposited on the inside of the sapphire cover windows. These optical coatings are the same as those mentioned previously and provide the dual functions of providing thermal protection and more resistance to radiation damage. Figure 11 is a repetition of the transmission curve of the optically coated cover window. In this figure, the

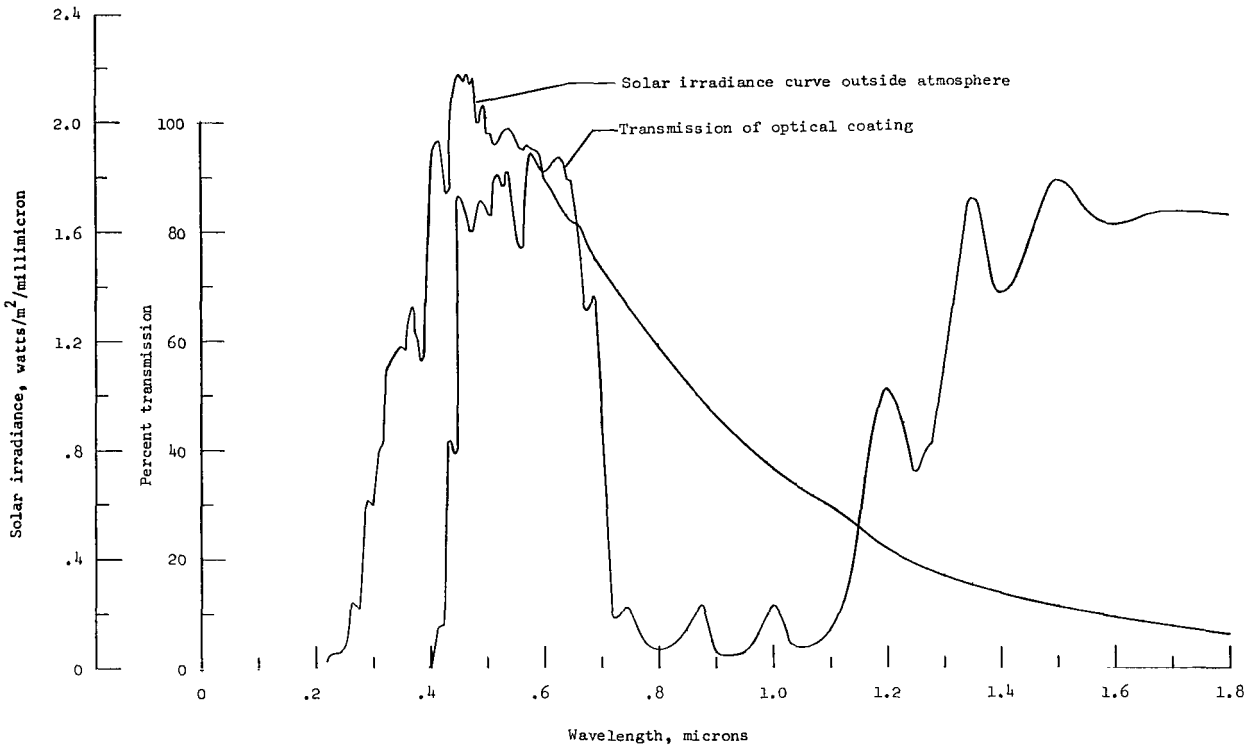

Figure 11.- Reduction of operating temperature of solar cells through the use of optical coatings.

transmission curve is superimposed upon the solar spectrum (ref. 8) to show that the optical coating reflects infrared solar radiation thus establishing a lower equilibrium temperature of the sensing elements. The actual amount of infrared radiation reflected by the optical coating is 65 percent. It should be noted that the absorption of the cover window and optical coating combination is less than 1 percent at all wavelengths longer than 0.45 micron. Thus, essentially, all the infrared solar radiation which is not transmitted by the window/coating combination is reflected so that no significant heat is generated within the cover window.

Launch Environment

The solar sensor described herein has been subjected to and has survived the extensive launch environmental testing summarized in table II. The test magnitudes were established by consideration of the available data on the past performance of the particular launch vehicle that was used by NASA's Spacecraft Orientation Control Systems Project and do not necessarily represent the maximum magnitudes that the sensor can withstand.

Figure 12 is a photograph of a single coarse sensing element. Figure 13 is a photograph of the parts of the fine sensor before assembly; and figure 14 shows the completely assembled fine sensor.

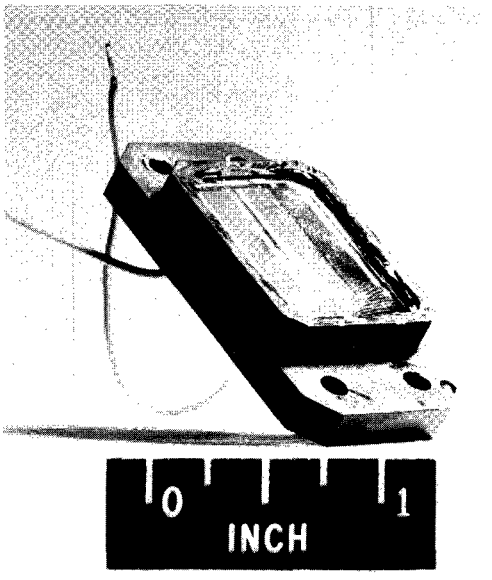

L-63-1711
Figure 12.- Single coarse sensing element.

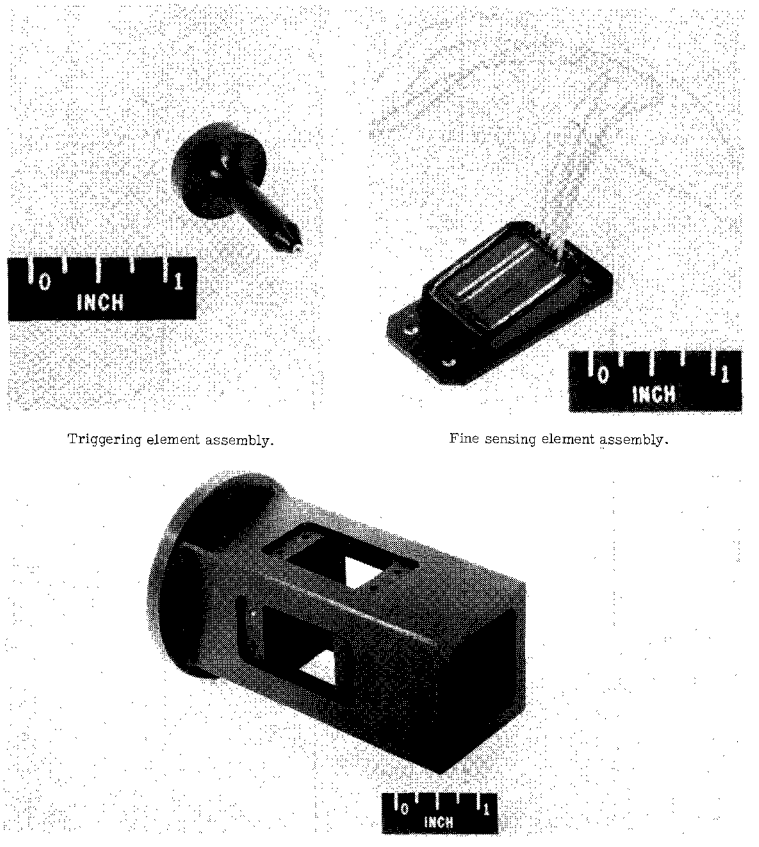

Triggering element assembly.

Fine sensing element assembly.

Fine sensor block.

L-63-9267
Figure 13.- Fine sensor parts before assembly.

The construction of the sensing elements is schematically illustrated in figure 15. Antireflection coatings are available which can be deposited on the outside of the cover window for the purpose of increasing the overall output of the silicon solar cells. The use of these antireflection coatings is not recommended, however, because of their exposure to direct ionizing radiation and resulting inherent degradation. The optical coating is protected by the sapphire window; thus, degradation of this coating is negligible for most space missions. The potting compound holds the components of the sensing elements in place and, because of its insulating properties, prevents rapid changes in the temperature of the sensing elements. A low-temperature-vulcanizing clear silicone potting compound (ref. 9) was chosen because of its proven resistance to discoloration when exposed to ultraviolet radiation (ref. 10). In order to reduce the discoloration of the potting compound, the optical coating was designed to reflect ultraviolet radiation as well as infrared radiation as is shown in figure 11. The thermistor shown in figure 15 is mounted in thermal contact with the center

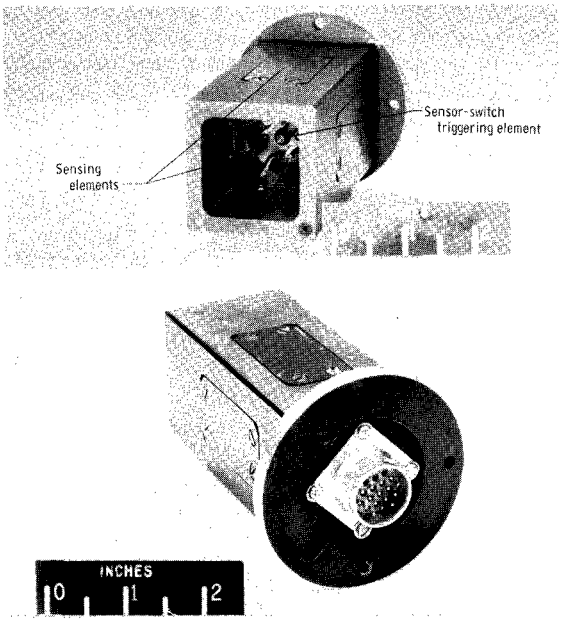

L-63-9268

Figure 14.- Two views of the completely assembled fine sensor.

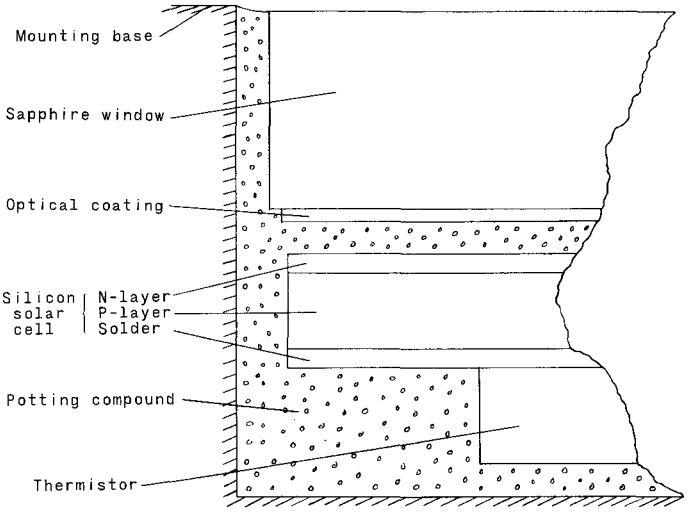

Figure 15.- Construction of sensing elements.

silicon solar cell of the sensing element and continuously monitors the temperature of that cell. Two of the four leads of the fine sensing element shown in figure 13 are attached to this thermistor.

As the mission requirements become more stringent, investigation of the degradation of the optical coating may become necessary. If future investigations should reveal that the degradation of the optical coating is significant, the problem can be eliminated by the omission of the optical coating. If the problem is solved by this method and if the overall radiation protection is considered to be marginal with respect to the mission under consideration, additional protection in the form of thicker shielding or more preirradiation will be necessary. If the optical coating is not used, the potting compound between the sapphire window and the solar cells must also be omitted since the potting compound will discolor rapidly without the ultraviolet protection supplied by the optical coating. An alternate approach is to retain only the ultraviolet reflecting portion of the optical coating along with the potting compound.

The discoloration and resulting decrease in transmission of the potting compound is an area which also needs further study in order to specify the long-term effect of the compound on the sensitivity of a solar sensor. If discoloration of the potting compound is discovered to be significant, the problem can be eliminated through the use of a construction technique which does not require the presence of a potting compound between the cover window and the solar cells. However, the latter construction technique has the following disadvantages: less structural strength; less insulation which will result in more rapid temperature variations in the sensing elements; loss of the heat conduction path from the solar cells to the window resulting in a higher operating temperature

for the sensing elements and a corresponding decrease in sensor sensitivity; and the loss of some protection from ionizing radiation. Tests in this laboratory have indicated that there is no significant difference, with respect to static acceleration, vibration, and shock, in the structural strength of sensing elements which were constructed with and without the potting compound between the protective window and the silicon solar cells. If, however, the protective window is struck by a projectile (a micrometeriod or a foreign object propelled by the pyrotechnic ejection of a heat shield, for example) of sufficient, and only sufficient, energy to break the window, laboratory tests have shown that the potting compound will both prevent the breakage of the solar cells and hold the broken window in place. Figure 16 shows the results of a test of comparative maximum temperature and rate of change of temperature which was made with two fine sensors, one with and one without potting compound between the window and cells. A photoflood lamp was used as the source of radiation, the pointing error was $0^{\circ} \pm 0.5^{\circ}$, and the temperatures shown are the average of readings taken from opposing thermistors.

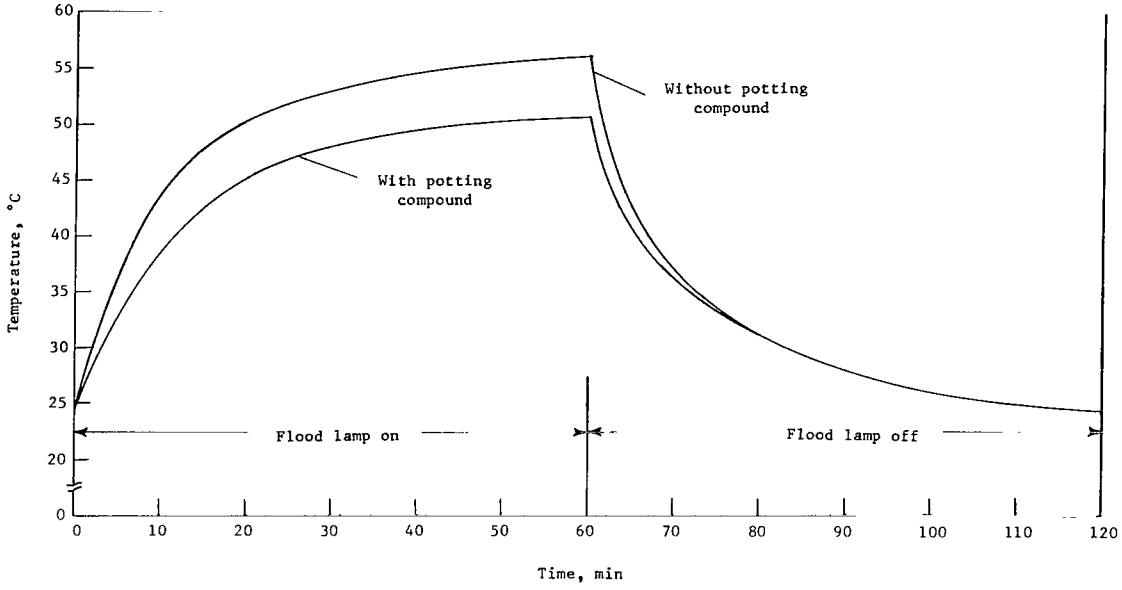

Figure 16.- Operating temperature of fine solar sensor with and without potting compound between window and cells.

CALIBRATIONS AND SPECIFICATIONS

A carbon arc solar simulator was used to obtain the solar sensor output curves presented in this section. A calibrated pyrheliometer was used to adjust the output of the solar simulator to one solar constant. The output of the solar simulator was continuously monitored and maintained at this level during the calibrations. The spectrum of the carbon arc simulator was not checked; but, to expose any significant errors in the solar sensor calibrations due to spectral mismatch, a check calibration was made with a spectrally calibrated mercury-xenon solar simulator. The check calibration obtained with the mercury-xenon simulator agreed within 10 percent with the calibration obtained

with the carbon arc simulator; the shapes of the two calibrations were the same.

Because of the inherent flicker of the carbon arc solar simulator, it was necessary to use the sun to obtain accurate small angle calibrations. The small angle calibrations were made at sea level on a clear day while the sun was near its local zenith. The stationary sensor was placed in the plane of the ecliptic and its output was continuously recorded, relative to an accurate time reference. Knowing the rate of revolution of the earth about its polar axis and the declination of the sun at the time of calibration, it was possible to convert the time reference of the sensor output to an angle reference. The solar radiation was monitored during the calibrations by a calibrated silicon solar cell, thus, the solar sensor output characteristics could be proportionately adjusted to an equivalent output at one solar constant (i.e., the amount of solar energy within the range of wavelengths to which the silicon solar cell responds was adjusted to a value equivalent to the solar energy present outside the earth's atmosphere and at 1 astronomical unit (1.5×10^{11} m) from the sun). After adjustment, the small angle calibration curves agreed within 15 percent with the calibration curves obtained by using the carbon arc simulator at the 0.5° and 1° points.

The accuracies quoted, relative to these solar sensor calibrations, are adequate since the primary objective was to investigate the shape and repeatability of the output curves. Figure 17 shows the single-axis calibration of the coarse sensor and the fine sensor calibrations are presented in figures 18, 19, 20, and 21.

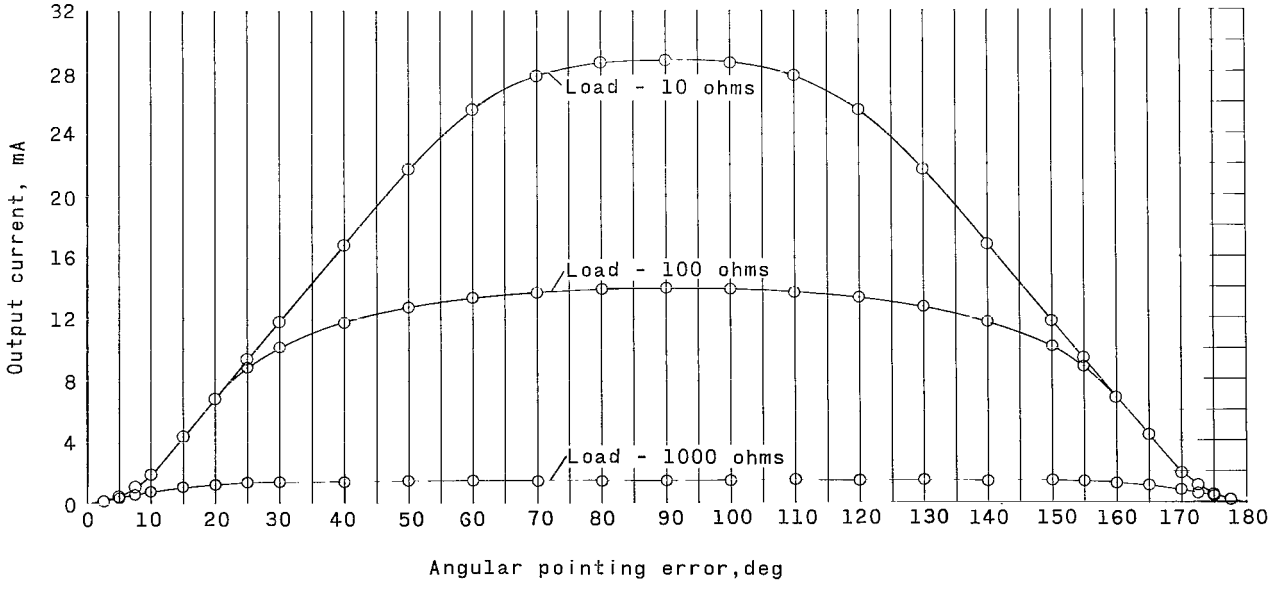

Figure 17.- Single-axis coarse sensor output calibration.

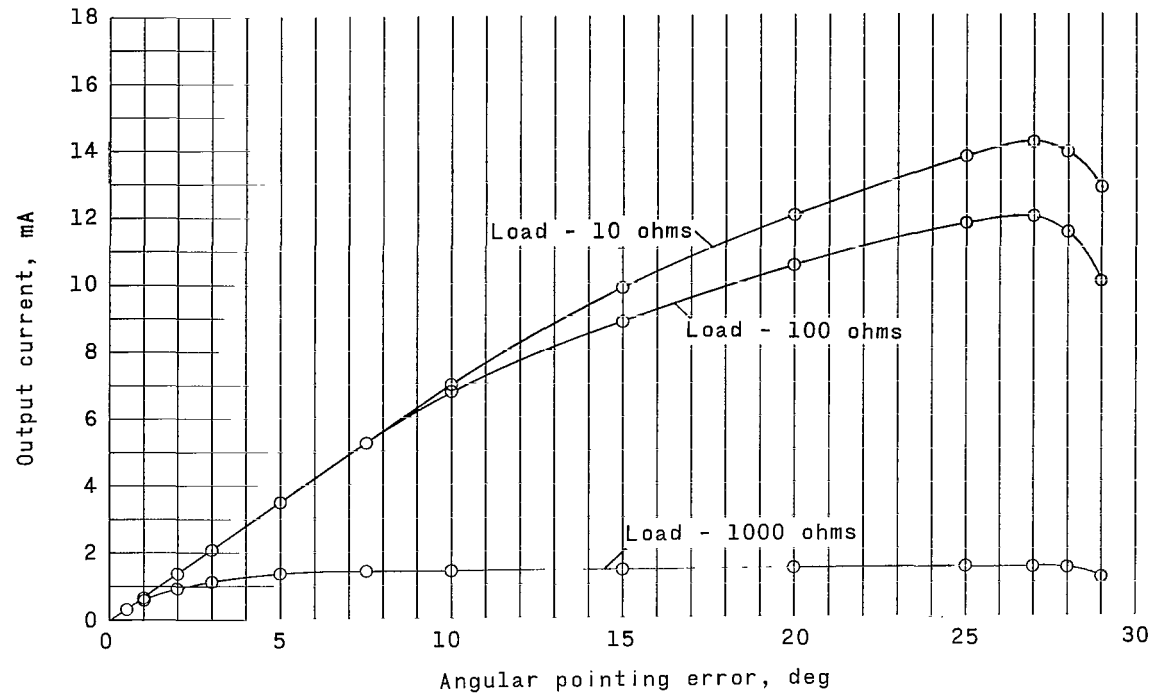

Figure 18.- Single-axis fine sensor output current calibration, $\alpha = 25^{\circ}$.

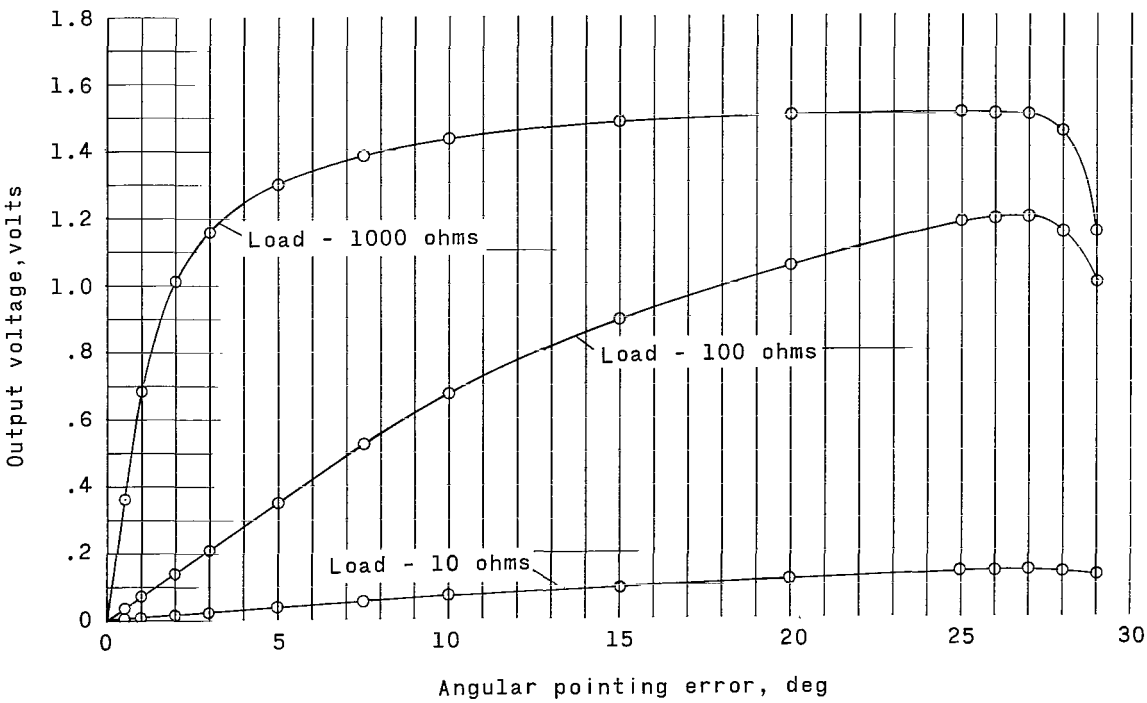

Figure 19.- Single-axis fine sensor output voltage calibration, $\alpha = 25^{\circ}$.

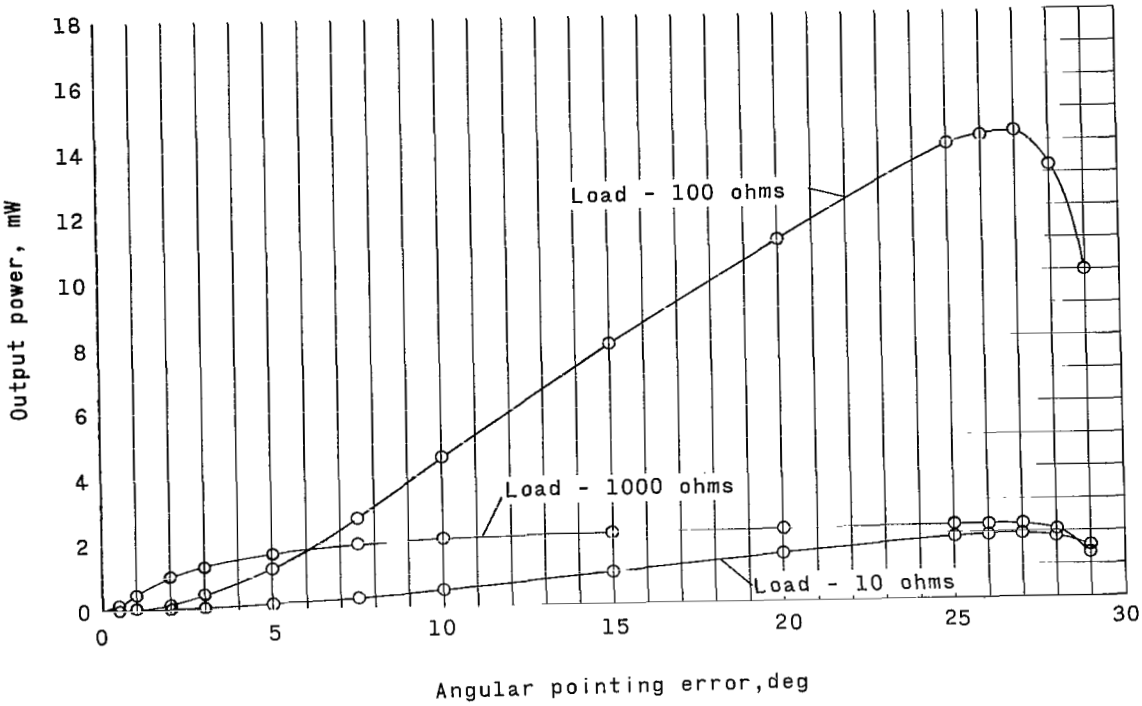

Figure 20.- Single-axis fine sensor output power calibration, $\alpha = 25^{\circ}$.

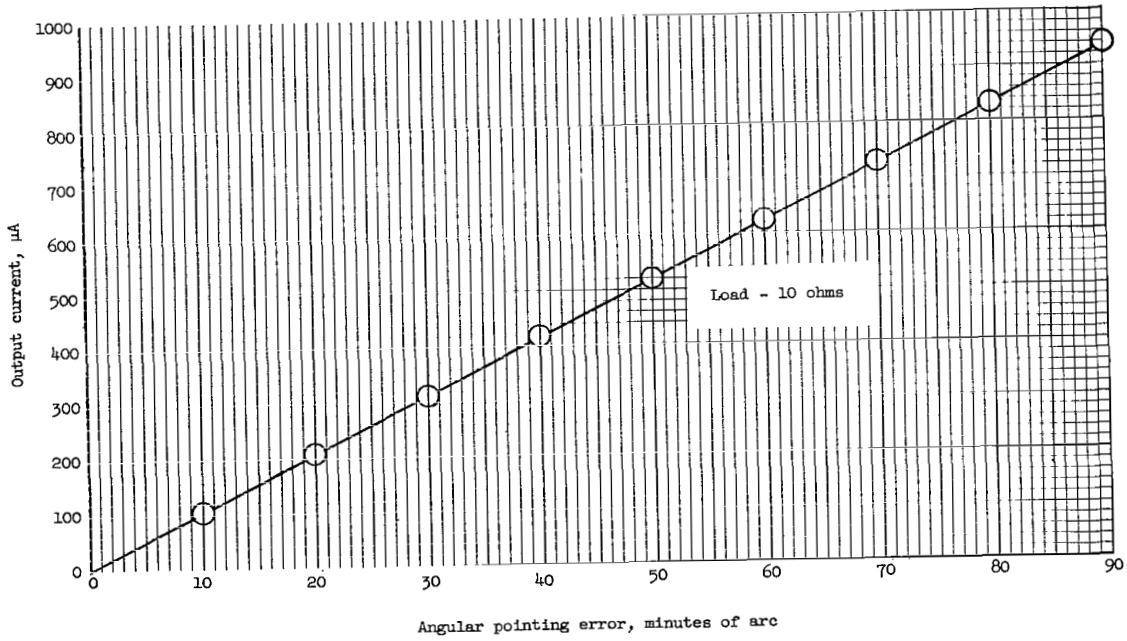

Figure 21.- Small angle fine sensor output current calibration, $\alpha = 25^{\circ}$.

The pertinent specifications of the fine and coarse solar sensors are summarized in table III. The weights given in table III are based on 2024-T4 aluminum structural material and the volumes given are the volumes of the parallelepipeds which will completely enclose each sensor.

The sensitivity of the fine solar sensor is a function of electrical load since the internal resistance of the silicon solar cell varies with illumination which causes the impedance match for maximum power transfer to vary with illumination also. Figures 18 and 19 reveal that, whereas the current output at small angular errors is relatively independent of load, the voltage output varies considerably with the load, and, as shown in figure 20, the maximum small angle sensitivity is obtained at high resistance loads. Figure 20 also shows that the maximum large angle sensitivity occurs at a load of the order of 100 ohms. The preceding statements lead to the conclusion that fine adjustment of the sensitivity of the sensor to a predetermined value within a specific error range can be accomplished by varying the load. Large increases in the sensitivity of the fine solar sensor can be obtained by simply increasing the number of solar cells that are connected in series to form the individual sensing elements. However, increases in sensitivity by this method are obtained at the expense of increased weight and volume of the sensor.

Reference to figure 18 will reveal that the angular range through which the fine sensor output is linear is also a function of the electrical load.

The angular pointing error at which control of the spacecraft is switched from the coarse sensors to the fine sensors has been established as 25°, as given in table III. A switching angle of 25° was established for the general purpose sensor to insure capture of the solar disk for any set of orbital parameters. If the initial orbit of the mission positions the spacecraft in continuous sunlight, the 25° switching angle may be necessary to insure capture of the solar disk. If, however, the initial orbit of the mission takes the spacecraft through the earth's umbra, capture of the solar disk will occur when the sun appears at the earth horizon at which time there is practically no pointing error induced by earth-reflected solar radiation. Under the latter conditions, the coarse sensors will be capable of effecting a capture maneuver to within a few degrees of the solar disk and the field of view of the fine sensor can be accordingly reduced. The preceding remains true even if the orbit of the spacecraft later becomes a continuous sunlight orbit.

The ability to reduce the fine sensor field of view to only a few degrees allows the sensitivity of the sensor to be increased significantly with only a small increase in weight. This increase in sensitivity is achieved by extending the shadow-box shield length as shown in figure 22. The increase in sensitivity occurs as a result of the fact that, at a given small angular pointing error, the area of one sensing element in the shadow of the shield has been increased, thus, the differential output of the sensing element pair is increased. (See ref. 2 and fig. 23.) The extended shadow-box method can certainly be applied to a sensor with any field of view with equal effectiveness, except that at large angular fields of view the extended shadow-box method of increasing the sensor

sensitivity becomes inferior to the method of additional cells in series with respect to weight and volume of the fine sensor.

Figure 24 shows that, depending upon the choice of load and angular range of interest, the variation in the output of the fine sensor with temperature can be significant. However, an accurate knowledge of the instantaneous temperature of the sensing elements and a complete family of temperature calibration curves will make it possible to take full advantage of the capability of the fine sensor to make angular measurements relative to the center of the solar disk regardless of the load chosen. The knowledge of the instantaneous temperature of the sensing elements is obtained through telemetry monitoring of the thermistors which are embedded in each sensing element. The required accuracy can be obtained by limiting the scale of the telemetry channel to a small range of temperature. The approximate operating temperature range of the sensor can be calculated for a particular set of orbital parameters.

It should be noted at this point that all of the desirable characteristics of the sensor cannot be attained simultaneously; thus, a compromise must be made. For example, if the fine sensor

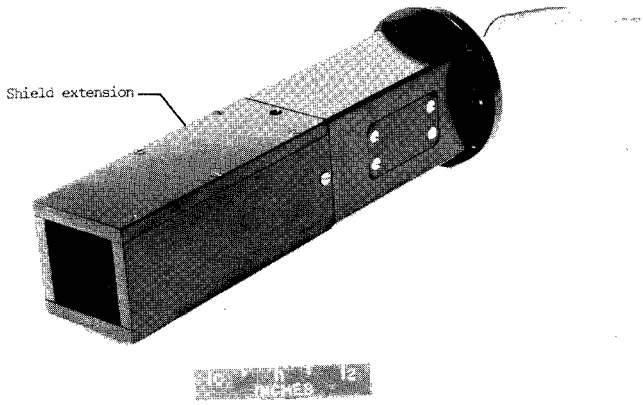

L-64-8471.1

Figure 22.- Fine solar sensor with extended shield.

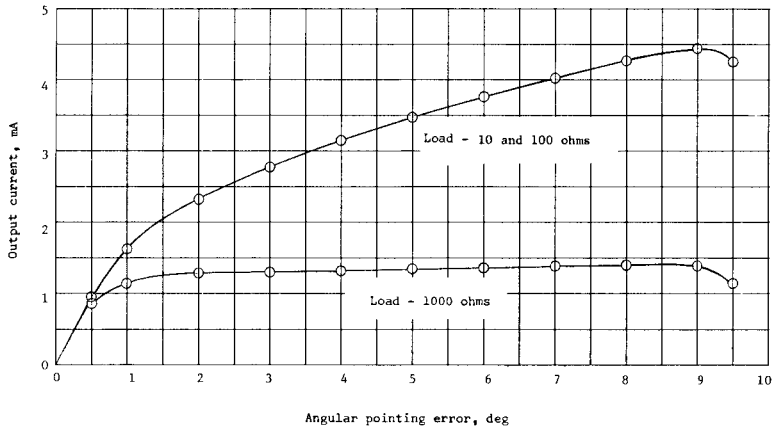

Figure 23.- Single-axis fine sensor output current calibration with extended shield, $\alpha = 8°$.

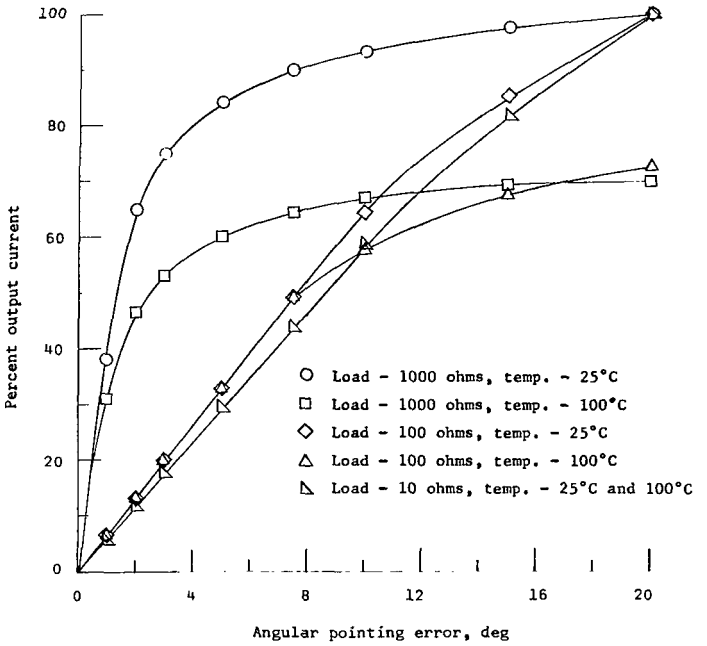

Figure 24.- Variation in fine sensor output with temperature (output current at an angular pointing error of 20° and a temperature of 25° C equals 100 percent).

is operated at a high resistance load, the following characteristics are present:

(1) High small angle sensitivity (see fig. 20)

(2) Restricted linear range (see fig. 18)

(3) Saturating output and restricted damping range (see fig. 18)

(4) Variation of output with temperature (see fig. 24)

(5) Maximum resistance to ionizing radiation damage (see fig. 10)

If the fine sensor is operated at a low resistance load, the following characteristics are present:

(1) Limited small angle sensitivity (see fig. 20)

(2) Extended linear range (see fig. 18)

(3) Nonsaturating output and extended damping range (see fig. 18)

(4) Output independent of temperature (see fig. 24)

(5) Limited resistance to ionizing radiation damage (see fig. 10)

The small angle repeatability of the fine sensor was established by making several small angle calibrations (see fig. 21) in rapid succession to insure

identical test conditions. The following results are based on the maximum deviation from the mean of 10 trials. At an error of 1 minute of arc the repeatability was ±2.4 seconds of arc (4.0 percent), and at an error of 1 degree of arc the repeatability was ±0.9 minute of arc (1.5 percent). The fact that the repeatability of the fine sensor is not a constant percentage of the instantaneous output may be an indication that a significant portion of the noise which limited the repeatability was introduced by random variation in atmospheric conditions.

The lifetime of the fine solar sensor, which is given in table III, is discussed in detail in the appendix.

CONCLUDING REMARKS

Photovoltaic solar sensors are, in general, inherently simple because they have no moving parts and require no power for operation other than the radiant energy obtained from the sun. The general purpose photovoltaic solar sensor, which has been described in this paper, is ruggedly constructed by unsophisticated techniques in order to maintain the inherent simplicity and thus to obtain excellent reliability. The general purpose solar sensor has been designed to meet the needs of a variety of space missions, and its flexibility allows it to be easily adapted to most attitude control systems.

The sensor accomplishes the dual functions of coarse and fine sensing. The four coarse sensing elements, when properly located on the spacecraft, have a full spherical field of view and the capability of capturing the solar target regardless of the initial orientation of the spacecraft relative to the sun-earth system. The fine solar sensor has a field of view which is restricted so that its pointing accuracy is unaffected by earth-reflected solar radiation. The sensitivities of the fine and coarse sensors can be adjusted to the optimum value through the proper choice of load; however, the adjustment of the sensitivity may involve several compromises with respect to other characteristics of the sensors. The repeatability of the fine solar sensor is ±2.4 seconds of arc at a pointing error of 1 minute of arc.

An inherent weakness of simple photovoltaic solar sensors is that they are susceptible to damage by the ionizing radiation of the space environment. Even though the degradation of the general purpose photovoltaic fine solar sensor has not been eliminated, it has been limited to a minimum value by the geometric design of the sensor, by the use of artificial sapphire cover windows, by the choice of the proper type of silicon solar cell, by the use of solar cells which have relatively high base material resistivities, by the use of optical coatings on the cover windows, by the proper choice of electrical load, and by the use of the technique of preirradiation of the solar cells. In addition, the possibility of null shift in the fine solar sensor due to asymmetrical degradation of opposing sensing elements has been decreased through the use of the technique of preirradiation matching of the silicon solar cells. Several of the techniques that make the solar sensor resistant to radiation damage reduce the maximum power output of the sensor which is equipped with a given number of cells; however, in the art of solar sensing, repeatability of the output over an extended

period of time is much more important than efficiency of operation. It is conservatively estimated that the fine solar sensor is capable of surviving the worst known space radiation environment for a period of 10 years with no more than 10-percent degradation.

Langley Research Center,
National Aeronautics and Space Administration,
Langley Station, Hampton, Va., November 16, 1965.

APPENDIX

CALCULATION OF EARTH-ORBIT LIFETIMES

Herein is calculated the approximate earth-orbit lifetime of the fine solar sensor for an assumed specific space mission. The following assumptions apply:

1. The earth orbit occupied by the assumed spacecraft is identical to the orbit of Telstar I: apogee, 3043 nautical miles (5630 kilometers); perigee, 512 nautical miles (947 kilometers); inclination, 44.8°.

2. The maximum tolerable degradation of the output of the fine solar sensor is 10 percent of its initial value.

3. The amount of preirradiation degradation of the sensor is (a) 0 percent, (b) 25 percent, and (c) 50 percent.

From figure 6, the 1 MeV electron radiation dose rate which is equivalent to that of the total radiation for the Telstar I orbit for a shielding of 1.57 g/cm^2 is 5.3×10^{11} electrons/cm^2/day or 1.9×10^{14} electrons/cm^2/year.

(a) From figure 9, the amount of 1 MeV electron radiation required to degrade the initial short-circuit current of the sensor by 10 percent (i.e., from 100 percent to 90 percent) is 1×10^{14} electrons/cm^2. Therefore, the orbital time required to degrade the sensor to 90 percent $I_{sc,o}$ is

$$\frac{1 \times 10^{14} \text{ electrons/cm}^2}{1.9 \times 10^{14} \text{ electrons/cm}^2\text{/year}} = 0.53 \text{ year}$$

The radiation damage protection afforded the sensor by the sapphire cover windows is included in this lifetime calculation. Also included is the resistance to radiation damage provided by preirradiation (zero percent in this case), N/P silicon solar cells, and 10 ohm-cm base material resistivity. The geometric design of the sensor, optical coatings, and electrical load also significantly affect the lifetime of the sensor. However, the effect of the electrical load will not be considered since this load will depend upon the requirements of each specific mission.

The above calculated lifetime is based upon the omnidirectional space radiation; the geometric design of the sensor block limits the space radiation to 6 percent of its omnidirectional value and gives a lifetime of

$$\frac{0.53}{0.06} = 8.8 \text{ years}$$

The optical coatings (see fig. 8) reduce the effective degradation of the sensor to 50 percent of the degradation which would occur without the use of the optical

coatings. Thus the lifetime now becomes

$$\frac{8.8}{0.5} = 17.6 \text{ years}$$

(b) From figure 9, the amount of 1 MeV electron radiation required to degrade the short-circuit current of the sensor by 10 percent (i.e., from 75 percent $I_{sc,o}$ to 67.5 percent $I_{sc,o}$) is

$$2.8 \times 10^{15} \text{ electrons/cm}^2 - 9 \times 10^{14} \text{ electrons/cm}^2 = 19 \times 10^{14} \text{ electrons/cm}^2$$

Therefore the orbital lifetime is

$$\frac{19 \times 10^{14} \text{ electrons/cm}^2}{1.9 \times 10^{14} \text{ electrons/cm}^2\text{/year}} = 10 \text{ years}$$

the geometrical design lifetime is

$$\frac{10}{0.06} = 167 \text{ years}$$

and the optical coating lifetime is

$$\frac{167}{0.5} = 334 \text{ years}$$

(c) From figure 9, the amount of 1 MeV electron radiation required to degrade the short-circuit current of the sensor by 10 percent (i.e., from 50 percent $I_{sc,o}$ to 45 percent $I_{sc,o}$) is

$$9 \times 10^{16} \text{ electrons/cm}^2 - 4 \times 10^{16} \text{ electrons/cm}^2 = 5 \times 10^{16} \text{ electrons/cm}^2$$

Therefore the orbital lifetime is

$$\frac{5 \times 10^{16} \text{ electrons/cm}^2}{1.9 \times 10^{14} \text{ electrons/cm}^2\text{/year}} = 263 \text{ years}$$

the geometrical design lifetime is

$$\frac{263}{0.06} = 4400 \text{ years}$$

and the optical coating lifetime is

$$\frac{4400}{0.5} = 8800 \text{ years}$$

The results of these calculations are presented in table IV for both the case which includes the protection supplied by the optical coating and the case which excludes the protection supplied by the optical coating, since, as stated in the body of the paper, it may be advantageous to omit the optical coating for certain missions. For comparison, the expected lifetimes of the two additional cases, in which the maximum tolerable degradation is 1 percent, are also presented in table IV. The lifetimes calculated may seem ridiculously high and the reader may wonder if all of the techniques for increasing the space lifetime of the sensor are really necessary. However, consideration of the following information will make it clear that design for the maximum lifetime is definitely in order. First, the space radiation data obtained by the various earth satellites over a period of years indicate that the radiation flux of the Van Allen Belts varies continuously by orders of magnitude. Second, although the Telstar I experiment is one of the best single sources of both ground and space semiconductor radiation damage data, it is somewhat limited in scope; this limitation results in the more than slight possibility of errors as large as orders of magnitude being introduced into the data presented in figure 6. The extrapolation of the Telstar I data in figure 6 will, of course, sustain the errors in the original data and could conceivably magnify the original errors. Third, the degradation of the sapphire cover window, the optical coating, and the optional potting compound has been neglected in the preceding calculations because of the lack of sufficient data to specify the effect of these degradations upon the lifetime of the sensor. As was stated in the body of this paper, these degradations may be significant.

In view of the large variations in the radiation flux of the Van Allen Belt, the possible inaccuracies in the data presently available on the in-space radiation damage of semiconductors, and the deficiency of data available on the radiation degradation of artificial sapphire, commercial optical coatings, and potting compounds, the general purpose solar sensor should be designed with safety factors of orders of magnitude. Based on the current state of the art, it is most conservatively estimated that a sensor can be designed which will degrade no more than 10 percent over a period of 10 years in the near earth space environment.

REFERENCES

1. Fontana, Anthony; Maynard, Julian D.; Brumfield, Marcus L.; and Parker, Otis J.: Flight Investigation of a Solar Orientation Control System for Spacecraft. NASA TM X-944, 1964.

2. Spencer, Paul R.: Study of a Solar Sensor for Use in Space-Vehicle Orientation Control Systems. NASA TN D-885, 1961.

3. Cooley, William C.; and Janda, Robert J.: Handbook of Space-Radiation Effects on Solar-Cell Power Systems. NASA SP-3003, 1963.

4. Brown, W. L.; Gabbe, J. D.; and Rosenzweig, W.: Results of the Telstar Radiation Experiments. Telstar I, NASA SP-32, Vol. 2, 1963, pp. 1505-1559.

5. Smits, F. M.: The Degradation of Solar Cells Under Van Allen Radiation. IEEE, Trans. Nucl. Sci., vol. NS-10, no. 1, Jan. 1963, pp. 88-96.

6. Cherry, William R.; and Slifer, Luther W.: Solar Cell Radiation Damage Studies With 1 MeV Electrons and 4.6 MeV Protons. NASA TN D-2098, 1964.

7. Baicker, J. A.; and Rappaport, P.: Radiation Damage to Solar Cells. Proc. Symposium on the Protection Against Radiation Hazards in Space. TID-7652, Book 1, U.S. Atomic Energy Commission, Nov. 1962, pp. 118-135.

8. Gast, P. R.: Solar Radiation. Handbook of Geophysics, Revised ed., The Macmillan Co., 1961, pp. 16-14 - 16-32.

9. Anon.: Silicones for Potting and Encapsulating. Tech. Data Book S-23A, Gen. Elec. Co.

10. Zoutendyk, John A.; Vondra, Robert J.; and Smith, Arvin H.: Mariner 2 Solar Panel Design and Flight Performance. Transcript of the Photovoltaic Specialists Conference. Vol. II - Report on Systems Experience, Applications, and Design, PIC-SOL 209/3.1, Interagency Advanced Power Group, July 1963, pp. A-1-1 - A-1-92.

TABLE I.- DOSAGE REQUIRED FOR SUCCESSIVE 10-PERCENT INCREMENTS OF 10 OHM-CM N/P SILICON SOLAR CELL DEGRADATION

Cell degradation	Dosage, 1 MeV electrons/cm^2
100 to 90 percent	1.0×10^{14}
90 to 80 percent	3.3×10^{14}
80 to 70 percent	1.5×10^{15}
70 to 60 percent	7.1×10^{15}
60 to 50 percent	3.1×10^{16}
50 to 40 percent	1.5×10^{17}
40 to 30 percent	6.8×10^{17}
30 to 20 percent	3.0×10^{18}
20 to 10 percent	1.4×10^{19}
10 to 0 percent	6.2×10^{19}

TABLE II.- ENVIRONMENTAL TEST MAGNITUDES

Test	Magnitude	
	Pitch and yaw axes	Roll axis
General vibration	±2g at 20 to 100 cps ±4g at 100 to 500 cps ±6g at 500 to 2000 cps	±4g at 20 to 100 cps ±14g at 100 to 500 cps ±28g at 500 to 2000 cps
Special vibration	±10g at 550 to 650 cps	±45g at 550 to 650 cps
Acceleration	160g	50g
Shock		30g for 10 milliseconds
Vacuum	10^{-7} millimeter of Hg	
Thermal	-50° C to 100° C, ambient	

TABLE III.- SPECIFICATIONS

Item	Fine sensor	Coarse sensor
Structural material	2024-T4 aluminum	2024-T4 aluminum
Weight	450g	88g
Volume	259 cm^3	46 cm^3
Sensing transducers	Silicon solar cells	Silicon solar cells
Type	N/P	N/P
Number per element	3	3
Size	2.0 cm by 0.5 cm	2.0 cm by 0.5 cm
Resistivity	10 ohm-cm	10 ohm-cm
Triggering element	1N2175 photoconductive diode	
Protective windows	0.15-cm-thick artificial sapphire	0.15-cm-thick artificial sapphire
Optical coating	See figure 11	See figure 11
Potting compound (optional)	Clear silicone	Clear silicone
Response time	20 microseconds	20 microseconds
General purpose:		
Switching angle	25°	
Sensitivity (100-ohm load)	0.7 mA/degree	
Linear range (100-ohm load)	$\pm 8^\circ$	
Special purpose (extended shield):		
Switching angle	8°	
Sensitivity (100-ohm load)	2.0 mA/degree	
Linear range (100-ohm load)	$\pm 1^\circ$	
Repeatability (Pointing error = 1 minute)	± 2.4 seconds	
Lifetime (10-percent degradation)	10 years (estimated)	

TABLE IV.- APPROXIMATE FINE SENSOR EARTH-ORBIT LIFETIMES

Case	Maximum tolerable degradation, percent	Preirradiation degradation, percent	Approximate lifetime, years	
			With optical coating	Without optical coating
a	10	0	18	9
b	10	25	334	167
c	10	50	8 800	4 400
d	1	50	500	250
e	1	75	20 000	10 000

NASA-Langley, 1966 L-4578

"The aeronautical and space activities of the United States shall be conducted so as to contribute . . . to the expansion of human knowledge of phenomena in the atmosphere and space. The Administration shall provide for the widest practicable and appropriate dissemination of information concerning its activities and the results thereof."

—NATIONAL AERONAUTICS AND SPACE ACT OF 1958

NASA SCIENTIFIC AND TECHNICAL PUBLICATIONS

TECHNICAL REPORTS: Scientific and technical information considered important, complete, and a lasting contribution to existing knowledge.

TECHNICAL NOTES: Information less broad in scope but nevertheless of importance as a contribution to existing knowledge.

TECHNICAL MEMORANDUMS: Information receiving limited distribution because of preliminary data, security classification, or other reasons.

CONTRACTOR REPORTS: Technical information generated in connection with a NASA contract or grant and released under NASA auspices.

TECHNICAL TRANSLATIONS: Information published in a foreign language considered to merit NASA distribution in English.

TECHNICAL REPRINTS: Information derived from NASA activities and initially published in the form of journal articles.

SPECIAL PUBLICATIONS: Information derived from or of value to NASA activities but not necessarily reporting the results of individual NASA-programmed scientific efforts. Publications include conference proceedings, monographs, data compilations, handbooks, sourcebooks, and special bibliographies.

Details on the availability of these publications may be obtained from:

SCIENTIFIC AND TECHNICAL INFORMATION DIVISION

NATIONAL AERONAUTICS AND SPACE ADMINISTRATION

Washington, D.C. 20546